

# Self-Induced and Progressive Photo-Oxidation of Organophosphonic Acid Grafted Titanium Dioxide

Nick Gys<sup>+</sup>,<sup>[a, b, j]</sup> Bram Pawlak<sup>+</sup>,<sup>[c]</sup> Kristof Marcoen,<sup>[d]</sup> Gunter Reekmans,<sup>[c]</sup> Leticia F. Velasco,<sup>[e]</sup> Rui An,<sup>[b]</sup> Kenny Wyns,<sup>[a]</sup> Kitty Baert,<sup>[d]</sup> Kaimin Zhang,<sup>[b]</sup> Léon Luntadila Lufungula,<sup>[f]</sup> Alessandra Piras,<sup>[g, h]</sup> Laurens Siemons,<sup>[f, k]</sup> Bart Michielsens,<sup>[a]</sup> Sabine Van Doorslaer,<sup>[i]</sup> Frank Blockhuys,<sup>[f]</sup> Tom Hauffman,<sup>[d]</sup> Peter Adriaensens,<sup>[c]</sup> Steven Mullens,<sup>[a]</sup> and Vera Meynen<sup>\*[a, b]</sup>

While synthesis-properties-performance correlations are being studied for organophosphonic acid grafted TiO<sub>2</sub>, their stability and the impact of the exposure conditions on possible changes in the interfacial surface chemistry remain unexplored. Here, the impact of different ageing conditions on the evolution of the surface properties of propyl- and 3-aminopropylphosphonic acid grafted mesoporous TiO<sub>2</sub> over a period of 2 years is reported, using solid-state <sup>31</sup>P and <sup>13</sup>C NMR, ToF-SIMS and EPR as main techniques. In humid conditions under ambient light

exposure, PA grafted TiO<sub>2</sub> surfaces initiate and facilitate photo-induced oxidative reactions, resulting in the formation of phosphate species and degradation of the grafted organic group with a loss of carbon content ranging from 40 to 60 wt%. By revealing its mechanism, solutions were provided to prevent degradation. This work provides valuable insights for the broad community in choosing optimal exposure/storage conditions that extend the lifetime and improve the materials' performance, positively impacting sustainability.

[a] N. Gys,<sup>+</sup> K. Wyns, B. Michielsens, S. Mullens, V. Meynen  
*Sustainable Materials*  
Flemish Institute for Technological Research (VITO NV)  
Boeretang 200  
2400 Mol (Belgium)  
E-mail: vera.meynen@uantwerpen.be

[b] N. Gys,<sup>+</sup> R. An, K. Zhang, V. Meynen  
*Laboratory of Adsorption and Catalysis (LADCA)*  
Department of Chemistry  
University of Antwerp  
Universiteitsplein 1  
2610 Wilrijk (Belgium)

[c] B. Pawlak,<sup>+</sup> G. Reekmans, P. Adriaensens  
*Analytical and Circular Chemistry (ACC)*  
Institute for Materials Research (IMO)  
Hasselt University  
Agoralaan 1  
3590 Diepenbeek (Belgium)

[d] K. Marcoen, K. Baert, T. Hauffman  
*Research Group Electrochemical and Surface Engineering (SURF)*  
Department Materials and Chemistry  
Vrije Universiteit Brussel  
Pleinlaan 2  
1050 Brussels (Belgium)

[e] L. F. Velasco  
*Department of Chemistry*  
Royal Military Academy  
Renaissancelaan 30  
1000 Brussels (Belgium)

[f] L. L. Lufungula, L. Siemons, F. Blockhuys  
*Structural Chemistry Group*  
Department of Chemistry  
University of Antwerp  
Groenenborgerlaan 171  
2020 Antwerp (Belgium)

[g] A. Piras  
*Laboratory of Applied Materials Chemistry*  
Unit of Nanomaterials Chemistry  
Department of Chemistry  
Namur University  
Rue de Bruxelles 61  
5000 Namur (Belgium)


[h] A. Piras  
*Design and Synthesis of Inorganic Nanomaterials (DESINE)*  
Institute for Materials Research (IMO-IMOMECA)  
Hasselt University  
Agoralaan 1  
3590 Diepenbeek (Belgium)


[i] S. Van Doorslaer  
*Laboratory of Biophysics and BioMedical Physics (BIMEF)*  
Department of Chemistry  
University of Antwerp  
Universiteitsplein 1  
,2610 Wilrijk (Belgium)

[j] N. Gys<sup>+</sup>  
Present address: Centre for Membrane Separations, Adsorption, Catalysis and Spectroscopy (cMACS), KU Leuven, Celestijnenlaan 200F, 3001 Leuven (Belgium)  
and  
Research Group Electrochemical and Surface Engineering (SURF), Vrije Universiteit Brussel, Pleinlaan Leuven, 2, 1050 Brussels (Belgium)

[k] L. Siemons  
Present address: Institute for Applied Chromatography (IAC), SGS Belgium NV, Polderdijkweg 16, 2030 Antwerp (Belgium)

[\*] These authors contributed equally

 Supporting information for this article is available on the WWW under <https://doi.org/10.1002/cplu.202200441>

 © 2023 The Authors. ChemPlusChem published by Wiley-VCH GmbH. This is an open access article under the terms of the Creative Commons Attribution Non-Commercial License, which permits use, distribution and reproduction in any medium, provided the original work is properly cited and is not used for commercial purposes.

## Introduction

The introduction of organic molecules onto the surface of metal oxides (e.g., TiO<sub>2</sub>, ZrO<sub>2</sub>, Al<sub>2</sub>O<sub>3</sub>, ZnO) through surface grafting provides the ability to tailor the surface properties towards an increased specificity and control of interactions. Such hybrid organic-inorganic materials are of importance in applications in which the performance is governed by interactions at the surface. In this context, the surface grafting of metal oxides with organophosphonic acids (PAs) and their derivatives is a promising method to tailor the surface properties relevant to a particular application.<sup>[1,2]</sup> Moreover, it allows (sub)monolayer coverages and control of the number and distribution of grafted organic groups, depending on the applied synthesis conditions such as the type of PA, the solvent, the temperature and the concentration.<sup>[3–6]</sup> Given the versatility of this grafting method, organophosphonic acid modified titania materials are of interest in a large variety of emerging applications and research domains such as membrane separation,<sup>[7,8]</sup> supported metal catalysis,<sup>[9,10]</sup> CO<sub>2</sub> conversion and adsorption,<sup>[11–13]</sup> hybrid (photo)electric devices,<sup>[14,15]</sup> biosensing<sup>[16,17]</sup> and selective metal sorption.<sup>[18,19]</sup>

Grafting of PAs comprises a complex set of reactions including the formation of Ti–O–P bonds via coordination of phosphoryl oxygen (P=O) to Lewis acidic sites, while P–OH groups are involved in condensation reactions with surface hydroxyl groups,<sup>[20]</sup> forming mono-, bi-, or tridentate binding modes. In reality, however, unravelling the precise surface chemistry of PA grafted titania materials is challenging, as multiple binding modes were found to coexist on the surface.<sup>[21,22]</sup> This is further influenced by the presence of hydrogen bonding and other non-covalent interactions within and between grafted PA groups, as well as with surface water.<sup>[21,23,24]</sup> Recent systematic studies on aliphatic and aromatic phosphonic acids<sup>[5,22,25]</sup> and aminopropylphosphonic acid<sup>[24]</sup> grafted TiO<sub>2</sub> demonstrate that a combination of experimental techniques and DFT calculations provides insights into the binding modes and surface conformations, as well as the interactions involved in their formation.

In the framework of materials performance and applicability, the stability and lifetime of the grafted organic layer are vital aspects to assess. Previous studies have already demonstrated the high hydrolytic stability of PA grafted metal oxides compared to organosilane-grafted groups.<sup>[26–28]</sup> These studies give a systematic overview of the impact of the alkyl chain length and type of PA on the hydrolytic stability of the grafted PAs in function of the pH by monitoring the loss of grafted organic groups upon increasing immersion time in aqueous conditions. However, only averaged macroscopic changes of the surface properties were determined, while in-depth post-mortem analysis was missing.

Only a few publications exist that report a more in-depth study of changes in the surface chemistry of PA modified TiO<sub>2</sub> surfaces upon ageing. These studies are limited to stability experiments under photocatalytic conditions via illumination of PA modified TiO<sub>2</sub> with UV light. Guerrero et al.<sup>[29]</sup> studied the stability of phenylphosphonic acid modified P25 towards UV

irradiation using <sup>31</sup>P-MAS NMR spectroscopy. They found that upon UV illumination in water, the initial <sup>31</sup>P resonance signals between 28–13 ppm decreased in intensity and a new signal appeared near 0 ppm. In toluene, however, only minor changes were observed in the <sup>31</sup>P-MAS spectra after UV illumination. While they assigned the newly formed phosphorus environment near 0 ppm to phosphate species, based on the <sup>31</sup>P-MAS spectra of orthophosphoric acid modified P25, further experimental proof and characterization of the illuminated samples were not provided.

Further systematic insights were provided by Kickelbick et al.<sup>[30]</sup> who compared the photocatalytic stability of TiO<sub>2</sub> modified with phenylphosphonic acid (PhPA) and dodecylphosphonic acid (DDPA). Monitoring the CH stretching and bending vibrations of DDPA and PhPA in FT-IR revealed a gradual decrease in intensity upon increasing exposure time to UV illumination, while the broad Ti–O–P absorption band practically remained unchanged. Hence, a degradation of the grafted organic groups was revealed while phosphate species remained present at the surface, as supported by <sup>31</sup>P-MAS NMR. Signals related to C–OH, C=O and O–C=O moieties were found in <sup>13</sup>C-CPMAS spectra after illumination. An oxidative degradation mechanism was put forward, which proceeds sequentially rather than via direct breakage of the P–C bond. However, the authors' assignment of <sup>13</sup>C NMR signals correlated to oxidized species originating from PA grafted groups might be questionable as modifications were performed in a methanol/water mixture (3:1) followed by washing with ethanol. Since alcohols are reported to adsorb both molecularly and dissociatively on TiO<sub>2</sub>,<sup>[31]</sup> these can potentially adversely contribute to the observed <sup>13</sup>C NMR signals.

Up to date, no in-depth studies are reported on the long-term stability of PA modified TiO<sub>2</sub> while exposed to ambient conditions (moist, ambient light) and general storage conditions of samples. Yet, in the many applications wherein PA modified TiO<sub>2</sub> materials are involved, such conditions are more frequently found rather than harsh exposure to UV light. Thus, since the performance of these materials is governed by specific surface interactions, changes in the interfacial surface chemistry have a possible influence on their performance in applications. Therefore, this work systematically elucidated the impact of short and long-term ageing conditions (humid versus dry, inert atmosphere) on the evolution of the surface properties of PA grafted TiO<sub>2</sub> (Hombikat M311). Using 3-aminopropylphosphonic acid (3APPA) and propylphosphonic acid (3PPA) as its amine-free analogue, and through grafting at two concentrations (20 and 150 mM), insights are provided on the impact of the amine group and the concentration on the ageing properties. Throughout a timeframe of 495 days, the surface properties of the grafted samples were monitored and characterized, in discrete time intervals, via a combination of complementary analytical techniques. Possible changes in the surface chemistry at the level of the phosphonate moiety and the carbon chain were investigated using solid-state <sup>31</sup>P-MAS NMR, ToF-SIMS and <sup>13</sup>C-CP-MAS NMR, providing detailed insights on the formed phosphorus- and carbon-based structures, thereby unravelling the corresponding ageing mechanism. Via Electron Paramag-

netic Resonance (EPR) measurements on the modified powders, experimental evidence was provided on how the charge-transfer properties are subject to the underlying origin of ageing. The peculiar role of water (in the form of moisture) and ambient light are highlighted, since they predominantly determined whether the original phosphonic acid-based chemistry was preserved or not. Furthermore, the influence of the titania support properties (e.g. crystal phase) on the ageing stability is evaluated via exposure of 3APPA grafted samples to different light sources in aqueous solution.

## Results and discussion

### First indications for ageing phenomena and structural changes

Elemental analysis (Table 1) on 3APPA and 3PPA modified Hombikat M311 showed a significant decrease in carbon content of 40–60% after 495 days of ageing under a humid atmosphere with 75% relative humidity. This is in agreement with changes in their DRIFT spectra, where the intensities of the signals in the stretching (3000–2800 cm<sup>-1</sup>) and deformation vibration (1470–1410 cm<sup>-1</sup>) regions of the propyl and aminopropyl chain decreased (Figure S.1). In contrast, no decrease in the nitrogen content was found after ageing within the experimental error (10%) of CHNS analysis. Similarly, the phosphorus content, as measured by ICP-OES analysis, revealed no changes after ageing with respect to the as-synthesized contents.

These results indicate a significant loss of organic groups from the surface. The absence of a concomitant decrease in nitrogen content suggests that the amine groups remained adsorbed at the surface via Lewis and/or Brønsted acid interactions. The occurrence of such drastic changes in elemental concentrations upon ageing under a humid atmosphere, without the presence of harsh degradation-promoting sources (e.g. UV), has not yet been reported in literature. In the next sections, the underlying possible changes in surface chemistry at the level of the phosphonate moiety and the carbon chain are discussed to elaborate on the ageing mechanism and the controlling parameters governing this ageing.

### Insights into the ageing mechanism at the level of the phosphonate moiety

#### Solid-state <sup>31</sup>P-MAS NMR

Although elemental analysis indicates no changes in the phosphorus content of the samples during ageing, insights into possible changes in the phosphorus environment are missing. Therefore, solid-state <sup>31</sup>P MAS spectra were recorded at regular time intervals of 3APPA and 3PPA modified Hombikat M311 upon ageing under a humid and dry-inert atmosphere. Pure 3APPA and 3PPA display sharp peaks at 25.1 and 37 ppm, respectively, as shown in Figure 1 (black solid line). Upon binding to the TiO<sub>2</sub> surface, a wide broadening is observed (spectra in blue), caused by the formation of different overlapping resonances. This can be assigned to the formation and coexistence of different binding modes (i.e., mono-, bi- and tridentate) and a wide variety of surface conformations and weak, non-covalent interactions (e.g. via H-bonds) of the organic groups, including interactions with bonded water.<sup>[24]</sup>

The NMR spectra of samples exposed for 4 days to a humid atmosphere, show changes in the relative intensities and chemical shifts of the overlapping resonance signals (spectra in red). An intensification of the signals at 21.6 and 26.4 ppm was observed for both 3APPA20 and 3PPA20, respectively. In addition, the main resonance of 3APPA20 shifts downfield from 25 ppm to 27.3 ppm while the main resonance of 3PPA20 shifts upfield from 32.5 ppm to 30.2 ppm. The same behavior could be observed in the samples modified with a higher phosphonic acid precursor concentration (150 mM), although in the case of 3PPA150 the effects were less pronounced because a sharp resonance is already present at 26.7 ppm (Figure S.2). Since the storage of the samples for 14 days under inert-dry conditions does not result in peak shifts or intensity changes with respect to the pristine <sup>31</sup>P-NMR spectra (Figure S.3), the aforementioned results reveal the sensitivity of the different phosphorus environments towards water.

After longer exposure times to humid conditions, gradual changes could be observed for all samples (Figure 2). The spectra are normalized to their total peak area to see the contribution of newly formed peaks. Firstly, an asymmetric peak with a main resonance around -2 ppm started appearing. This was accompanied by a small downfield signal at 7 ppm, a downfield shoulder at 0 ppm and an upfield signal at -15 ppm. In parallel with the formation of these new signals, the intensity of the main pristine peaks between 40–19 ppm decreased gradually. This observed trend upon ageing was identical for all

**Table 1.** Overview of C, N and P concentrations of as-synthesized (0 days) and in 75% humidity aged (495 days) 3APPA and 3PPA modified Hombikat M311. Experimental error of <sup>1</sup>10% and <sup>2</sup>5%.

Sample	C [%] <sup>1</sup>			N [%] <sup>1</sup>		P [%] <sup>2</sup>	
	0 days	495 days	% decrease	0 days	495 days	0 days	495 days
3APPA150	1.01	0.57	44	0.37	0.35	1.20	1.20
3PPA20	1.45	0.63	57	n.a.	n.a.	n.d.	n.d.
3PPA150	1.70	0.97	43	n.a.	n.a.	1.37	1.30

n.a. = not applicable, n.d. = not determined

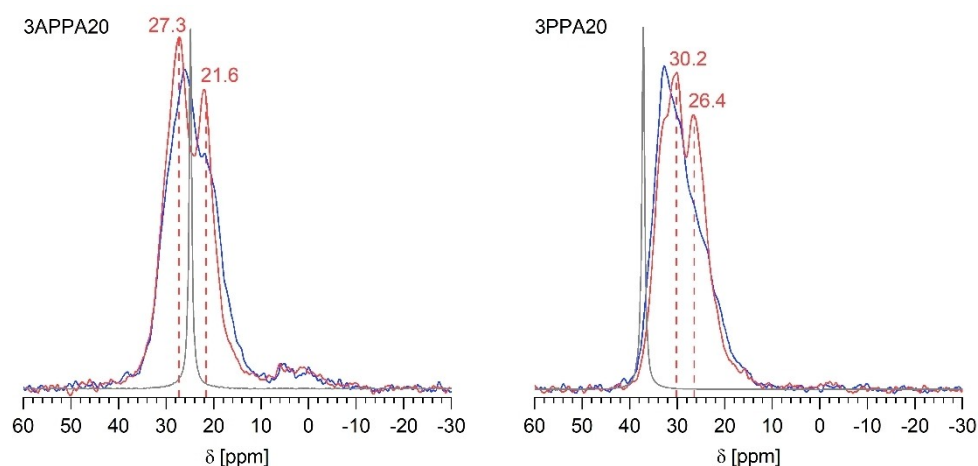


**Figure 1.** Solid-state  $^{31}\text{P}$  MAS NMR of 3APPA20 and 3PPA20 after synthesis (blue spectra) and after 4 days of contact to a humid atmosphere (red spectra). The spectra of the pure phosphonic acid precursors are also shown (grey solid lines). The influence of water on the spectra was apparent from the perceived intensity changes and peak shifts.

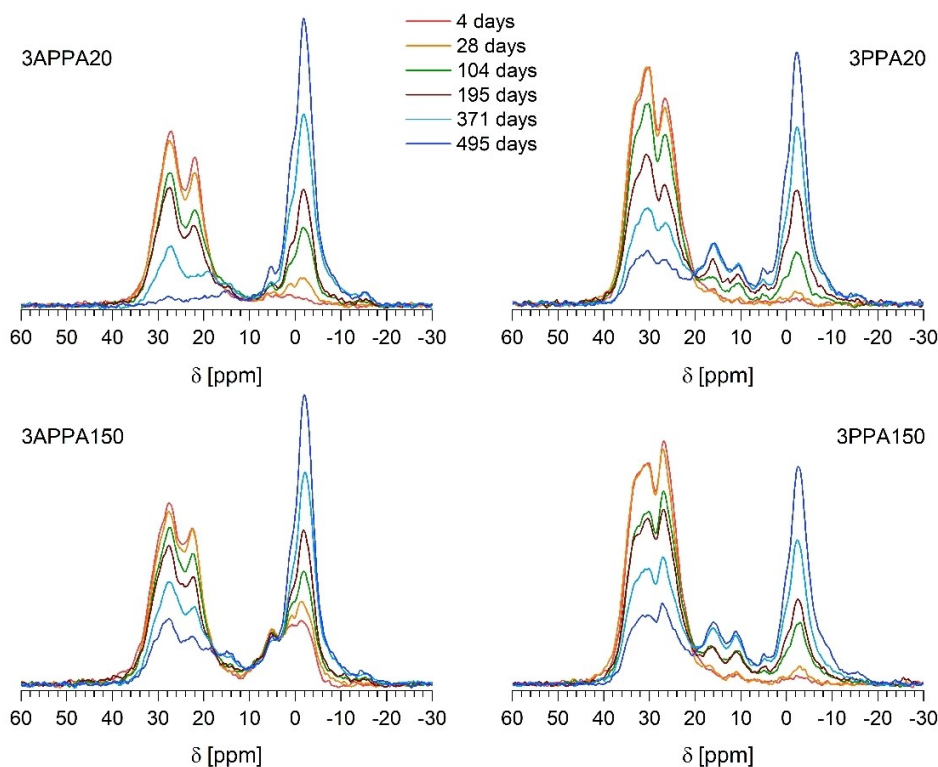


**Figure 2.** Solid-state  $^{31}\text{P}$ -MAS NMR spectra of 3APPA20, 3APPA150, 3PPA20 and 3PPA150 at different exposure times (4–495 days) under a humid atmosphere.

samples, and thus, irrespective of the used phosphonic acid precursor and modification concentration. This suggests the occurrence of similar changes in surface chemistry upon ageing in a humid atmosphere for 3APPA and 3PPA grafted powders, despite the differences in the  $^{31}\text{P}$ -NMR spectra of freshly grafted 3APPA and 3PPA. In addition, 3PPA grafted powders also display prominent increasing peaks at 18 and 11 ppm upon ageing which are less obvious for the 3APPA grafted powders. In contrast, under dry-inert conditions, the formation of these new phosphorus environments upon ageing was absent (Fig-

ure S.4 and S.5). Small changes only start to appear after 195 days of storage, compared to after 28 days under humid conditions. To exclude the role of oxygen, ageing was performed under dry air instead of a dry  $\text{Ar}/\text{N}_2$  atmosphere. However, no changes were found during this long-term ageing under dry air, as exemplified by 3APPA20 in Figure S.6, suggesting that oxygen does not play a role in the ageing process. Hence, these results clearly illustrate that humidity plays a fundamental role in the ageing process.

In order to investigate the rate of ageing, two different regions were defined: region 1 encompasses the chemical shifts that were present in the pristine grafted powders, while region 2 was indicative of the newly formed environments. Region 1 for 3APPA ranges from 40 to 10 ppm, and region 2 from 10 to -20 ppm. For 3PPA, regions 1 and 2 were taken from 40 to 20 ppm, and from 20 to -20 ppm, respectively. Upon plotting the ratio of the peak areas of region 2 and region 1 in function of the ageing time, a linear change was observed, indicating a systematic change with time (Figure S.7). The slope of the linear fits can be used to estimate the rate of change in the grafted powders. The rate of change in descending order was  $3APPA20 > 3PPA20 > 3PPA150 > 3APPA150$ . Since the presence and adsorption of water at the surface plays a role in the ageing, differences in surface coverage of grafted groups influenced the number of surface adsorption sites for water,<sup>[32]</sup> and thus could be responsible for the difference in the susceptibility towards ageing. For example, modification degrees of 0.6 and 0.8 groups/nm<sup>2</sup> were obtained for 3APPA20 and 3APPA150, respectively. The authors would like to point out that these values do not represent saturation-behavior, but rather can be clarified by the selected modification conditions and the presence of amine-surface interactions. For a detailed discussion, the reader is referred to Table S.1. Experimental evidence of an increased hydrophobicity with increasing precursor concentration is revealed by water adsorption measurements (Figure S.8). Between relative humidities from 0 to 35%, a relatively lower water uptake in the adsorption branch was found for 3APPA150. Since this part of the isotherm is specifically related to the surface chemistry, this indicated the lower water affinity of 3APPA150 compared to 3APPA20. In addition, as it was reported that 3APPA was involved in conformations in which the aminopropyl chains were folded back towards the surface,<sup>[24]</sup> these groups could sterically shield or block adsorption sites for water. This shielding was illustrated by quantum chemical calculations of 3APPA adsorption on the anatase 101 facet (Figure S.9). The slower rate and inferior ageing after 495 days for 3APPA150 might therefore also be ascribed to the larger area of water adsorption sites that were shielded.

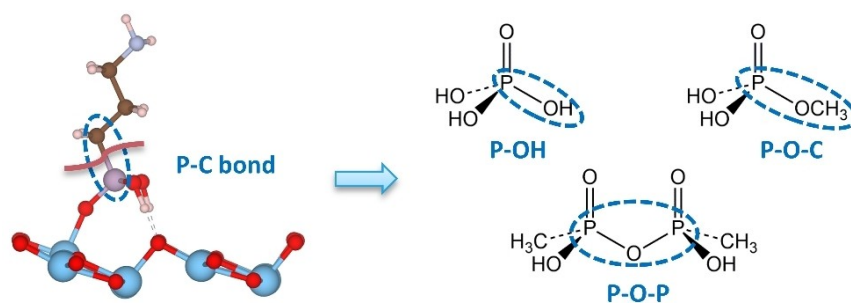


**Figure 3.** Non-limitative schematic overview of plausible phosphorus-based structures formed during ageing in a humid atmosphere via breakage of the P–C bond in an organophosphonic acid bonded/adsorbed group, illustrated by monodentate 3APPA on anatase (101).

### Modification with phosphorus-based structures and associated <sup>31</sup>P NMR spectra

The newly formed signals during ageing in a humid atmosphere between -15 and 7 ppm in the <sup>31</sup>P-MAS NMR spectra, with a predominant signal around -2 ppm, indicated distinct structural changes at the level of the phosphonate anchor group. Possible functionalities at this position include phosphates, phosphate mono-, di-, and triesters (P–O–C bonds) and pyrophosphonates (P–O–P bonds), as schematically shown in Figure 3.

In order to identify the formed structures upon ageing that could be allocated to the -2 ppm signal, the studied TiO<sub>2</sub> Hombikat M311 powder was modified with precursors representing different classes of phosphorus-based structures: i) orthophosphoric acid (oPA, H<sub>3</sub>PO<sub>4</sub>), ii) potassium dihydrogen phosphate (PDHP, KH<sub>2</sub>PO<sub>4</sub>) as phosphate, iii) a monomethyl-dimethylphosphate mixture (MM-DMP) and trimethylphosphate (TMP) as organophosphate derivatives and iv) dipropylidiphosphonic acid (DPDPA) as pyrophosphonate. Unfortunately, no conclusive statements on the prevalence of either structure upon ageing could be made. All results were compiled in the supplementary information, including Figure S.10 and S.11.

### Insights into the formed phosphorus structure(s) via ToF-SIMS

ToF-SIMS measurements were performed to gain further insight into the changes induced during ageing, focusing on characteristic ion fragments for 3APPA and 3PPA modified Hombikat M311 that increased or decreased in relative intensity during ageing. In the case of 3APPA20, CN<sup>-</sup> (*m/z* = 26.02) and C<sub>3</sub>H<sub>9</sub>NPO<sub>3</sub><sup>-</sup> (*m/z* = 138.08) were characteristic ion fragments in the negative ToF-SIMS spectra, while C<sub>3</sub>H<sub>7</sub>O<sup>+</sup>, C<sub>2</sub>H<sub>4</sub>O<sub>2</sub><sup>+</sup> and C<sub>3</sub>H<sub>10</sub>N<sup>+</sup> were characteristic in the positive ToF-SIMS spectra. C<sub>3</sub>H<sub>9</sub>NPO<sub>3</sub><sup>-</sup> was an interesting fragment because it corresponds to the “molecular ion minus 1 hydrogen” (M–H)<sup>-</sup>. Figure 4A1 shows how this (M–H)<sup>-</sup> mass peak decreased from the as-synthesized state to ageing for 257 and 495 days in humid conditions, giving first indications on structural changes of the 3APPA grafted groups upon ageing which is in line with the earlier presented NMR results. In addition, similar decreasing trends were visible for the CN<sup>-</sup> and C<sub>3</sub>H<sub>10</sub>N<sup>+</sup> fragments, as

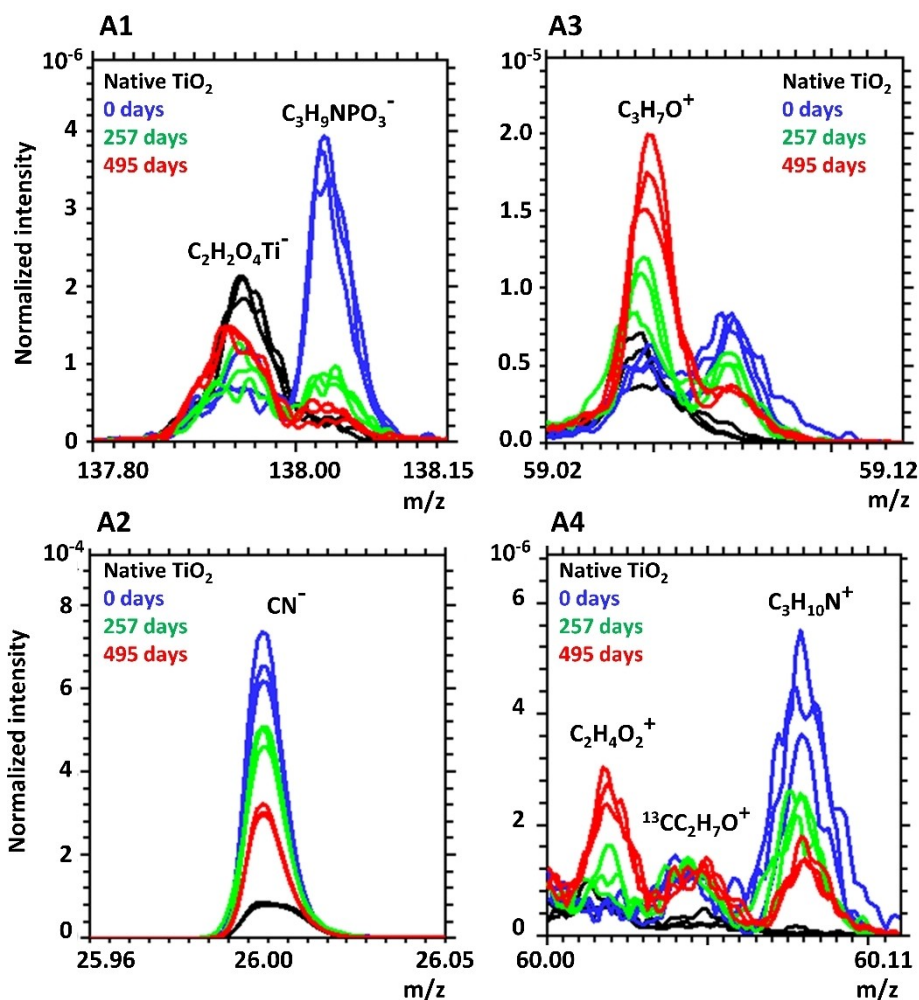


**Figure 4.** Evolution of characteristic ion fragments in ToF-SIMS for native Hombikat M311 (black) and 3APPA20 after synthesis (blue) and upon ageing under a 75% humid atmosphere for 257 days (green) and 495 days (red). (A1)  $\text{C}_3\text{H}_9\text{NPO}_3^-$ ; (A2)  $\text{CN}^-$ ; (A3)  $\text{C}_3\text{H}_7\text{O}^+$ ; (A4)  $\text{C}_2\text{H}_4\text{O}_2^+$  and  $\text{C}_3\text{H}_{10}\text{N}^+$ . All overlays show 3 spectra per condition. Intensities were normalized to the total ion intensity.

shown in Figures 4A2 and 4A4, respectively. Although elemental analysis revealed no decrease in the nitrogen content upon ageing, the decreasing  $\text{CN}^-$  signal confirms changes at the level of the amine functionality. This might be associated with the breakage of the C–N bond in the aminopropyl chain, although other factors resulting in such a decrease cannot be ruled out (e.g. differences in fragmentation due to conformation changes of 3APPA or interactions of the nitrogen atom with the surface). Besides the decreasing relative intensities of  $\text{C}_3\text{H}_9\text{NPO}_3^-$ ,  $\text{CN}^-$  and  $\text{C}_3\text{H}_{10}\text{N}^+$  fragments, an increasing relative intensity of  $\text{C}_3\text{H}_7\text{O}^+$  (Figure 4.A3) and  $\text{C}_2\text{H}_4\text{O}_2^+$  (Figure 4.A4) is found upon ageing for 3APPA20.

Based on the trends in these characteristic fragments, ToF-SIMS confirmed structural changes and fragmentation of the 3APPA grafted groups upon ageing, involving the oxidation of the carbon chain. Similar results were obtained for 3PPA grafted Hombikat M311 (Figure S.12), revealing a decrease in relative intensities of the  $\text{C}_3\text{H}_8\text{PO}_3^-$  ( $m/z=123.07$ ) and  $\text{C}_3\text{H}_6\text{PO}_2^-$  ( $m/z=105.05$ ) fragments. Similarly to 3APPA20, the occurrence of oxidation reactions is confirmed by the appearance and

intensity increase of  $\text{C}_3\text{H}_7\text{O}^+$  and  $\text{C}_2\text{H}_4\text{O}_2^+$  fragments upon ageing. For a summarizing overlay of the negative ToF-SIMS spectra in the mass range 0–200  $m/z$  for native Hombikat M311 and as-synthesized 3APPA20 and 3PPA20, the reader is referred to Figure S.13.

In order to identify the newly formed phosphorus structure(s) upon ageing, as revealed by  $^{31}\text{P}$  NMR, characteristic phosphorus-containing fragments in ToF-SIMS spectra of  $\text{TiO}_2$  modified with oPA, MM-DMP and DPDPA (Figure S.14) were compared with the ToF-SIMS spectra of aged 3APPA20 and 3PPA20 (Figure S.13). Analysis of the DPDPA reference precursor powder revealed characteristic  $\text{P}_2\text{O}_4^-$  ( $m/z=125.95$ ) and  $\text{P}_2\text{O}_5\text{H}^-$  ( $m/z=142.95$ ) ion fragments assigned to P–O–P bonds, while in the ToF-SIMS spectra of aged 3PPA20, these fragments were not found (Figure S.15). Secondly, analysis of MM-DMP modified  $\text{TiO}_2$  showed  $\text{CH}_4\text{PO}_4^-$  ( $m/z=111.01$ ) and  $\text{CH}_3\text{O}^-$  ( $m/z=31.03$ ) as characteristic ion fragments (Figure S.16). However, fragments in the form of  $\text{C}_x\text{H}_y\text{PO}_4^-$  and  $\text{CH}_3\text{O}^-$  were not present in the spectra of aged 3PPA20. Hence, one can conclude that pyrophosphonate (P–O–P) and organophosphate (P–O–C)

related structures were not formed upon ageing. Considering the list of possible candidates accounting for the signal around  $-2$  ppm, this suggests that the ageing was likely to be characterized by the formation of phosphate species.

Figure S.13 shows an overlay of mass spectra obtained for aged 3APPA20 and 3PPA20 modified  $\text{TiO}_2$  powders in red, and for oPA modified  $\text{TiO}_2$  powder in green. Evaluating changes in the relative intensities of the  $\text{PO}_2^-$ ,  $\text{PO}_3^-$ ,  $\text{TiPO}_4^-$  and  $\text{TiPO}_5^-$  ion fragments, which are characteristic of the interaction between  $\text{TiO}_2$  and phosphorus-based structures, enables to deduce possible changes at the phosphonate moiety during ageing. oPA150 revealed relatively higher  $\text{PO}_3^-/\text{PO}_2^-$  and  $\text{TiPO}_5^-/\text{TiPO}_4^-$  intensity ratios compared to the respective intensity ratios in the aged 3APPA20 and 3PPA20 samples. However, if one compares the aged samples (Figure S.13, red spectra) with as-synthesized 3APPA20 and 3PPA20 modified samples (Fig-

ure S.13, blue spectra), increasing relative intensities of the  $\text{PO}_3^-$  and  $\text{TiPO}_5^-$  fragments were found. In Figure 5, the intensity ratios  $\text{PO}_3^-/\text{PO}_2^-$  (Figure 6A) and  $\text{TiPO}_5^-/\text{TiPO}_4^-$  (Figure 6B) were plotted for 3APPA20 and 3PPA20. In both cases, an increase was observed, indicating that oxidation of the phosphonic acid group took place.

In conclusion, through a combination of ToF-SIMS and NMR on a set of reference materials, it was possible to link aged 3APPA and 3PPA modified powders to the formation of phosphate species. Further indications on the formation of phosphate species were given by the O1s XPS spectra of 3APPA20 and 3APPA150 after 365 days of ageing. The reader is referred to the appendix (Table S.2 and Figures S.17–S.18) for a detailed discussion and interpretation of the spectra.

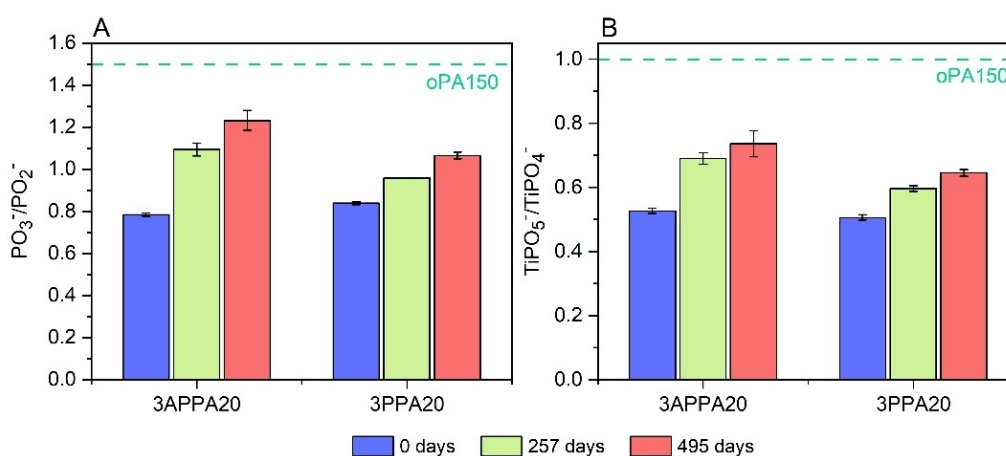


**Figure 5.** (A) Intensity ratio of  $\text{PO}_3^-/\text{PO}_2^-$  fragments in ToF-SIMS, plotted for as-synthesized powders (0 days) and 3APPA20 and 3PPA20 aged for 257 and 495 days. (B) Intensity ratio of  $\text{TiPO}_5^-/\text{TiPO}_4^-$  fragments in ToF-SIMS, plotted for as-synthesized powders (0 days) and 3APPA20 and 3PPA20 aged for 257 and 495 days.

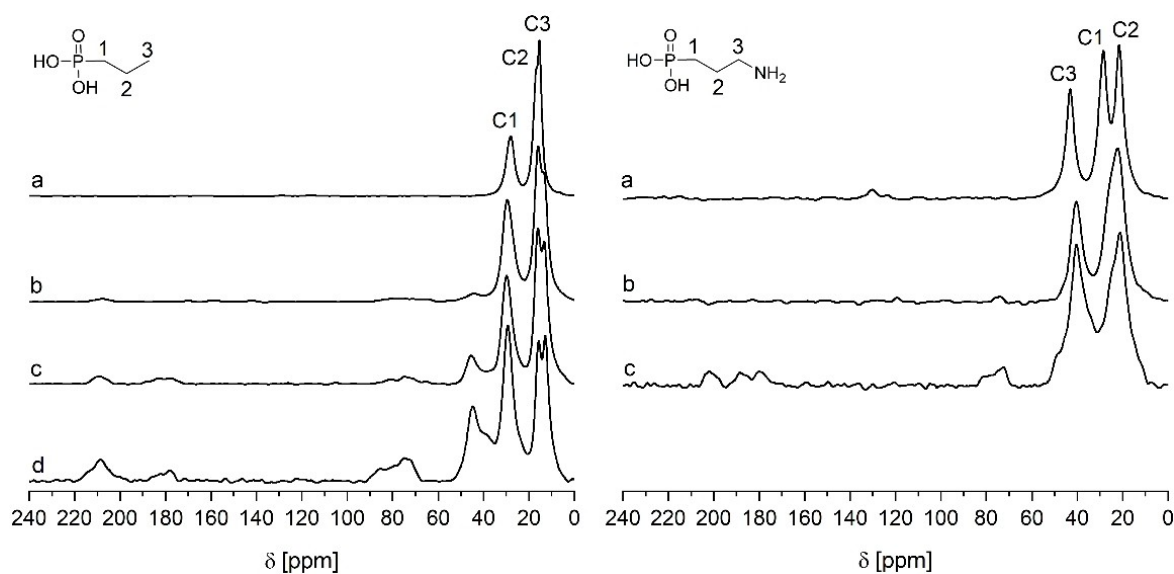


**Figure 6.** Solid-state  $^{13}\text{C}$ -CPMAS NMR spectra of 3PPA150 (left) and 3APPA150 (right). The pure precursor (a), as-synthesized modified powders (b) and the modified powders after exposure under a humid atmosphere for 371 days (c) and for 495 days (d) were recorded.

## Insights into the ageing mechanism at the level of the aminopropyl- and propyl chain

Solid-state  $^{31}\text{P}$ -NMR and ToF-SIMS measurements already revealed that the as-synthesized  $\text{R-PO}_3$  moieties were involved in oxidation reactions during ageing in a humid atmosphere, resulting in the transformation to  $\text{PO}_4$  structures. Insights into the ageing mechanism and structural changes at the level of the carbon chain were provided by  $^{13}\text{C}$  CPMAS NMR measurements. Figure 6 compares the evolution of the  $^{13}\text{C}$  CPMAS spectra for 3PPA150 and 3APPA150 during ageing. Based on a liquid-state  $^{13}\text{C}$ -APT (attached proton test) spectrum of the pure 3PPA precursor (Figure S.19), the signals at 28, 17 and 15 ppm could be assigned to carbon atoms C1, C2 and C3 of the propyl chain, respectively. The APT spectrum of the pure 3APPA precursor allowed to assign the signals at 43, 28 and 21 ppm to the C3, C1 and C2 carbon atoms of the aminopropyl chain. (Figure S.20).

After 371 days of ageing for 3PPA150 (Figure 6c), a distinct peak appeared at 35–45 ppm together with minor peaks between 85–60 ppm and 215–170 ppm. Strong similarities were found with 3APPA150, where the 45–35 ppm signal was present as a shoulder on the C3 signal and where the other newly formed carbon signals were more visible. The 85–60 ppm region could be assigned to the presence of alcohol or ether groups, while the 215–170 ppm region was consistent with carbonyl carbons in aldehydes and ketones (215–190 ppm) and carboxylic acids (<190 ppm). In the case of 3APPA, the coexistence of amides besides carboxylic acids cannot be excluded. The assignment of the 45–35 ppm region was more ambiguous as it could represent either branched hydrocarbons or alpha carbon atoms in carbonyl moieties ( $\text{C-C=O}$ ). Upon further ageing up to 495 days for 3PPA150 (Figure 6d), the changes became more pronounced. The 45–35 ppm signal further increased in intensity, and, given the concomitant increase with the 215–170 ppm signals, the former signal was likely to be assigned to alpha carbon atoms. This assignment was further supported by solid-state  $^1\text{H}$  wPMLG MAS spectra, that revealed a new shoulder at 2.5 ppm on the broad band between 2–0 ppm originating from the aliphatic hydrogen atoms for 3PPA150 aged for 495 days (Figure S.21). This chemical shift region could be assigned to hydrogens attached to carbons that were bonded to  $\text{sp}^2$ -hybridized carbons as in carbonyl moieties ( $\text{H-C-C=O}$ ).<sup>[33]</sup> Upon ageing, the signals of the alcohol groups (85–60 ppm) also showed a significant increase in intensity. Given the decrease in carbon content observed from elemental analysis and the formation of carboxylic acids during ageing for 3APPA and 3PPA, the release of  $\text{CO}_2$  from decarboxylation reactions might be the origin of this decrease.

The formation of oxidized carbon groups upon ageing is in line with the ToF-SIMS results (Figure 4). This is further supported through DRIFT spectra of modified 3APPA and 3PPA, by the presence of new signals between  $1730\text{--}1670\text{ cm}^{-1}$  superimposed on the broad and intense absorption band of molecularly adsorbed water (Figures S.22–S.23 and Table S.3). These signals were characteristic for  $\text{C=O}$  stretching vibrations

of aldehydes, ketones and/or carboxylic acids,<sup>[34]</sup> which was in agreement with the  $^{13}\text{C}$ -CPMAS NMR results. A detailed in-depth discussion of the changes in the DRIFT spectra upon ageing is beyond the scope of this work, and the reader is referred to the SI.

In addition, the results of the water vapour sorption isotherms (Figure S.8) also confirmed the oxidation of the 3APPA modified samples during their exposure to humidity. This was deduced from the gradual increase in the slope of the water adsorption branch at relative humidities between 0–35% with the time of storage for both concentrations (20 and 150 mM). This trend indicated the formation of species with higher affinity for water, such as hydroxyl, carbonyl and/or carboxylic groups. A more detailed discussion is presented in the SI. Remarkably, these phenomena only took place when the samples were exposed to a humid atmosphere and not under dry-inert conditions. When looking at possible underlying mechanisms, photocatalytic reactions come to mind, as the samples were exposed to ambient light. Indeed, the occurrence of phosphate ( $\text{PO}_4^{3-}$ ) formation, associated with the cleavage of  $\text{P-C}$  bonds, coinciding with oxidation reactions and a decrease in carbon content, in combination with the absence of changes in the surface chemistry in air, indicates a radical mechanism involving water which could be related to the photocatalytic activity of  $\text{TiO}_2$ . The higher activity of PA modified  $\text{TiO}_2$  in interfacial charge-transfer reactions was experimentally evidenced by EPR measurements (Figure 7). Under high vacuum at room temperature, 3APPA and 3PPA modified Hombikat M311 showed clear EPR signals between 341–347 mT, while a reference sample (i.e. a blanc modification reaction of Hombikat M311 under the same conditions without the addition of PA) was EPR silent. The  $g$ -tensor components of these EPR signal patterns, as derived from spectral simulations (Table 2), were consistent with  $\text{O}_2^-$  species adsorbed at the surface.<sup>[35]</sup> These transient species were formed via electron transfer from surface  $\text{Ti}^{3+}$  centers to adsorbed  $\text{O}_2$  molecules. These radicals are formed and persist under vacuum. Under air, these signals are usually quenched, due to different reasons: (i) the dipolar interaction with the paramagnetic  $^3\text{O}_2$  leads to signal broadening, and (ii) the highly reactive surface species will rapidly react with other molecules, such as water (Figure S.24).

Similar results were obtained on a 3APPA and 3PPA modified P25 support (Figure S.25). Although these  $\text{Ti(IV)-OO}^-$  radicals were only observed under high vacuum exposure, these results provide experimental evidence that the PA modification of  $\text{TiO}_2$  surfaces intrinsically resulted in an activation of charge transfer reactions and the formation of transient radical species, which was not present in the unmodified supports.

**Table 2.** Principal  $g$ -tensor values of the paramagnetic  $\text{Ti(IV)-OO}^-$  species determined from the simulations of the EPR spectra of 3APPA and 3PPA grafted M311 (Figure 7, dashed lines). Experimental error:  $\pm 0.001$

Parameters	$g_1$	$g_2$	$g_3$
M311_3APPA	2.023	2.009	2.002
M311_3PPA	2.022	2.009	2.003



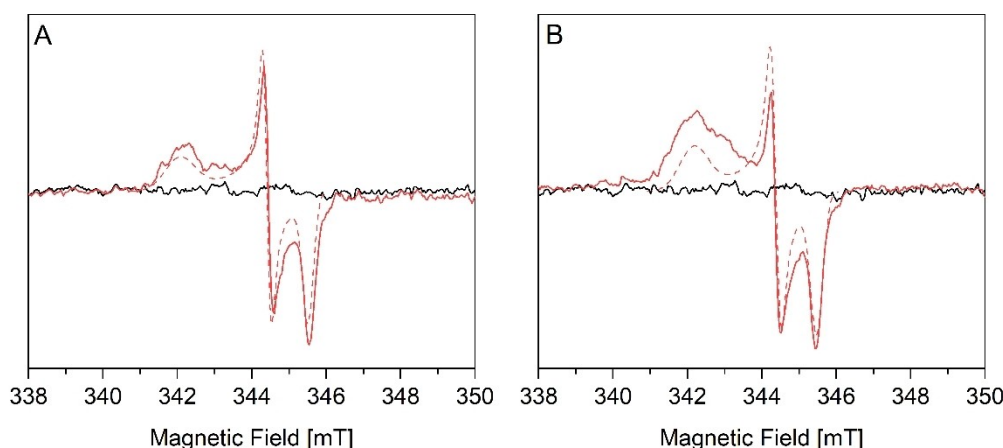


**Figure 7.** X-band CW EPR spectra of 3APPA grafted Hombikat M311 (A) and 3PPA grafted Hombikat M311 (B), recorded under high vacuum ( $< 10^{-4}$  mbar) at room temperature with a microwave power of 2 mW. Red: modified powder, black: blank modification without the addition of phosphonic acid. Dashed line: simulation using parameters in Table 2.

### Influence of the support properties and illumination conditions

The synergy between the photocatalytic active anatase phase, the presence of water (both adsorbed and in vapour phase) and ambient light are thought to be the cause for the degradation and oxidation reactions. To unambiguously reveal this synergy, ageing experiments were conducted under different illumination conditions for aqueous dispersions of 3APPA modified samples at a concentration of 20 mM. The experiments in dark conditions were conducted as reference experiments, since it was previously reported that  $\text{TiO}_2$  was able to retain some photocatalytic activity in the absence of illumination due to the prior accumulation of reactive oxygen species (ROS) under ambient light exposure.<sup>[36]</sup>

Two  $\text{TiO}_2$  supports were selected to evaluate if the ageing was proportional to their photo-oxidation properties: Hombikat M311 (anatase) and  $\text{TiO}_2$  rutile. Based on literature, anatase is

generally considered to have a distinctly higher photocatalytic activity than rutile, even though the band gap of rutile (3.0 eV) is smaller than that of anatase (3.2 eV).<sup>[37]</sup> Based on UV-VIS measurements (Figure S.26), a bandgap of 3.24 and 3.27 eV was found for native and 3APPA modified Hombikat M311, respectively, indicating that PA grafting did not alter the electronic band structure of the powder.

Stirring of the grafted materials in water under constant illumination, resembling harsh ageing conditions, quickly led to major changes in the  $^{31}\text{P}$  MAS spectra (Figure 8). The total peak area of the spectra was normalized to evaluate the contribution of newly formed peaks. Firstly, the  $^{31}\text{P}$ -NMR spectra of the pristine 3APPA grafted supports were compared. As already shown in Figure 2, the broad asymmetric band between 35 and 10 ppm of 3APPA grafted anatase consists of a main resonance at 25 ppm and an upfield shoulder around 22 ppm. The main resonance of pristine 3APPA grafted rutile resembled that of pristine 3APPA grafted anatase. However, the signal was

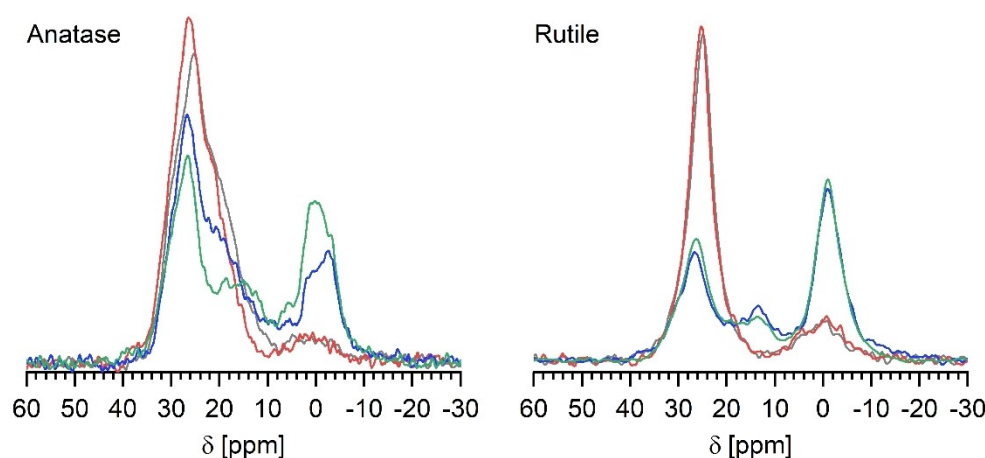


**Figure 8.** Solid-state  $^{31}\text{P}$  MAS NMR spectra of 3APPA modified anatase and rutile powder after stirring for 12 days in  $\text{H}_2\text{O}$  under different (illumination) conditions. Native (grey), dark (red), ambient light (blue) and UV-light (green).

sharper (35–15 ppm) than that of anatase (35–10 ppm) and lacks the upfield shoulder around 22 ppm which suggests a more uniformly grafted layer. In addition, a broad band consisting of multiple signals was present between 10 and –10 ppm for each support upon modification with 3APPA.

In the following paragraph, the impact of the different illumination conditions and corresponding changes in the  $^{31}\text{P}$ -NMR spectra are discussed and evaluated between the two supports. Stirring in the dark (red spectra) results in negligible changes compared to the  $^{31}\text{P}$  spectra of the pristine grafted powder for each support, confirming the requirement of light and thus photo-activation in the degradation mechanism. Upon exposure of grafted anatase to ambient light (blue spectrum), an asymmetric broad band appears in the region between 10 and –10 ppm, composed of at least two overlapping signals at 0 and –2 ppm and the appearance of a signal around 7 ppm. This coincides with a decrease in intensity of the pristine peaks between 35 and 10 ppm. A further increase and decrease in intensity of both regions, respectively, was observed under UV illumination (green spectrum). These chemical shifts were in agreement with the long-term ageing under humid conditions (Figure 2) and, combined with the stronger changes under UV illumination, this supports the occurrence of oxidative degradation reactions via photochemical reactions.

Since  $^{31}\text{P}$ -NMR and  $^1\text{H}$ -NMR measurements showed that the phosphonic acid precursors were themselves not sensitive to UV degradation (Figure S.27–S.30), the support must play an important role. Illumination of 3APPA grafted rutile revealed similar changes as for anatase in the decrease of the pristine signals (35–15 ppm) and the intensity increase between 10 and –10 ppm, characterized by a symmetric band centered at –2 ppm. Interestingly, rutile clearly displayed a relatively stronger intensity increase in the latter region compared to anatase for either ambient- and UV light illumination, since there was no significant difference in their  $^{31}\text{P}$  spectra. Since anatase is known to possess a higher photocatalytic activity than rutile, this suggests that the degradation of the grafted phosphonic acid moieties to phosphate groups is not directly proportional to the intrinsic photocatalytic activity of the unmodified support. It hints at distinct differences between 3APPA modified anatase and rutile in terms of interactions with water and/or at differences in surface activation (energy) upon modification.

The origin and peak assignment of the broad band between 10 and –10 ppm upon grafting was challenging since the contribution of species different from phosphate and formed via other mechanisms than photocatalytic oxidative degradation could not be excluded. For example, besides photochemical reactions, the formation of a layered aminopropylphosphonate phase at the surface via a dissolution-precipitation reaction could not be excluded. For the grafting of titania, such a phase was typically formed when modifications were performed in water where its presence increased with increasing temperatures and PA concentrations.<sup>[3,6,29]</sup> Indeed, this would also explain the higher intensity of the broad band consisting of multiple signals between 10 and –10 ppm observed for pristine 3APPA150 (Figure S.2) compared to

3APPA20 (Figure 1). Moreover, the presence of the amine group seems to enhance the formation of phosphorus environments in this 10 and –10 ppm region, since for neither 3PPA20 (Figure 1) nor 3PPA150 (Figure S.2), such signals were present upon modification. Additionally, to assess the potential contribution of ambient light during modification on the in-situ  $\text{PO}_4$  formation, 3APPA150 was synthesized in dark conditions. However, this only resulted in a slightly lower intensity of the 10 to –10 ppm environment (Figure S.31), illustrating that the contribution of other structures (e.g. layered aminopropylphosphonate) than phosphate species could not be excluded or that other ageing mechanisms than the one reported are contributing to the formation of phosphate species.

In order to evaluate the importance of the  $\text{TiO}_2$  photocatalytic properties on the oxidative degradation, the comparison was made with 3APPA modified  $\text{ZrO}_2$  powder (CZE-G1, ZirPro). It was hypothesized that  $\text{ZrO}_2$ , possessing a wider bandgap of 5.07 eV (Figure S.26), would be less sensitive to photo-oxidative degradation compared to  $\text{TiO}_2$ . However,  $^{31}\text{P}$  MAS NMR of pristine 3APPA modified zirconia already revealed an intense broad band between 10 and –10 ppm (Figure S.32), complicating the origin and peak assignments of this region since the formation of other species, different from phosphate or other degradation mechanisms besides photo-oxidative reactions, could not be excluded, as discussed earlier. It would require a further systematic and in-depth study to unravel the origin of the additional contribution(s) of other phosphorus structures or ageing mechanisms on this  $^{31}\text{P}$  chemical shift region, which was beyond the scope of this work.

### Underlying properties and mechanism governing degradation

The results obtained in this study are intriguing in the sense that P–C bonds were known for their high stability under ambient conditions in the absence of enzymatic or microbial activity. The formation of a  $\text{PO}_4$  structure at the surface upon ageing in a humid environment, either in the vapour- or liquid phase, implies the incorporation of an oxygen atom during cleavage of the P–C bond. Of the many reactive oxygen species that could be formed at the titania surface during photocatalytic reactions, such as  $\cdot\text{OH}$ ,  $\text{O}_2^-$ ,  $\text{H}_2\text{O}_2$ ,  $\text{Ti-O}\cdot$ , hydroxyl radicals have been regarded as the most active species that govern photocatalytic reactions.<sup>[38,39]</sup> Surface hydroxyl groups (Ti–OH) have been reported to play an important role in the separation and surface diffusion of electron-hole ( $e^-/h^+$ ) pairs. Especially, the formation of hydroxyl radicals has commonly been regarded to be initiated through the oxidation of Ti–OH groups or/and surface adsorbed  $\text{H}_2\text{O}$  by photogenerated holes ( $h^+$ ), resulting in surface bonded  $\cdot\text{OH}$  or mobile  $\cdot\text{OH}$  radicals.<sup>[40]</sup> Interestingly, PA modification seems to have a negligible impact on the band gap energy, as revealed by the comparison between native and 3APPA modified Hombikat M311 (anatase) in UV-VIS measurements (Figure S.26). Therefore, other surface properties introduced upon grafting should be governing the observed photo-induced ageing phenomena.

Previous studies, combining the use of experimental and computational techniques, revealed that the first layer of surface adsorbed water was essential in facilitating the hole-trapping ability of titania surfaces, thereby promoting the charge transfer between  $h^+$  and  $H_2O$ .<sup>[41–43]</sup> It was shown that an enhancement of the photocatalytic reaction rate was directly correlated to the number of hydrated surface Ti–OH groups by hydrogen bonding with water. Moreover, the photocatalytic activity of  $TiO_2$  was reported to be enhanced via surface modification with phosphates or orthophosphoric acid, which can be ascribed to the introduction of Brønsted acid/base sites that enable the formation of strong hydrogen bonds with water.<sup>[41,44]</sup> One could rationalize that this is different in the case of organophosphonic acid modified  $TiO_2$ , where, due to the presence of organic groups, an increased hydrophobicity was observed in water sorption measurements compared to native  $TiO_2$  (Figure S.8A).

An explanation for this relatively high photocatalytic activity could thus be found in studies evaluating the interaction between water and organophosphonic acid modified  $TiO_2$  surface at the molecular level. Recently, Van Dijck et al.<sup>[32]</sup> studied the water desorption behaviour of propyl- and phenylphosphonic acid P25 via an in-depth IR study at different hydration degrees to reveal the nature and strength of interaction between water and the modified surface. Their results showed that polymeric water chains interact more weakly on a modified surface compared to native P25, which was in line with the decrease in hydrophilicity. However, the signals related to molecularly adsorbed water and surface hydroxyl groups on the modified surfaces persisted upon progressive heating, while these signals already disappeared for P25 at the same conditions. Supported by DFT calculations of the water adsorption on unmodified and modified anatase (101), this indicated that the first water layer interacts more strongly with a modified surface, owing to the presence of hydrogen-bonded networks between water, surface hydroxyl groups and P–OH groups. Hence, this could rationalize the ageing mechanism and the initiation of photo-induced oxidation reactions already under ambient light. These oxidation reactions result in the observed progressive degradation of the propyl- and aminopropyl chain of 3PPA and 3APPA, respectively, characterized by the formation of alcohol groups as intermediary products followed by a subsequent increase in oxidation state by the formation of ketone, aldehyde and carboxylic acid groups. Lastly, first indications were obtained that the observed ageing phenomena could be extended to other  $TiO_2$  supports and types of PAs. For 3-aminopropyl and 6-aminohexylphosphonic acid modified  $TiO_2$  P25, similar changes were observed in  $^{31}P$  NMR in the appearance of an intense band between 10 and  $-10$  ppm upon ageing for 300 days (Figure S.33). Also the solvent used during modification seemed to influence the ageing mechanism, since 3PPA modified sol-gel  $TiO_2$  revealed that the relative intensities of the newly formed signals in DRFT upon ageing, depending on whether water or toluene was used as solvent (Figure S.34).

## Conclusions

This study reports the unexpected phenomenon of irreversible changes in the surface chemistry of organophosphonic acid (PA) grafted  $TiO_2$  and the role of water and ambient light herein. It highlights the importance of storage conditions to preserve the surface properties of phosphonic acid modified titania. Throughout a timespan of two years of storage under humid and dry conditions, the surface chemistry of PA grafted  $TiO_2$  (Hombikat M311) samples was monitored and characterized by a combination of analytical techniques. Under humid conditions, the initial phosphonate chemistry was gradually converted to phosphate species via progressive oxidation reactions, while oxidation reactions at the carbon chain resulted in the formation of alcohol groups and carbonyl/carboxylic moieties. This was accompanied by a strong decrease in the carbon content, and hence, loss of organic functionality. However, the Ti–O–P bonds remain unaffected, confirming its reported high hydrolytic stability. Interestingly, exposure to inert and/or dry conditions maximizes the stability of the material in preserving the initial surface chemistry upon grafting. The results revealed that only a combination of exposure to humid conditions and ambient light was limiting to the lifetime of the materials. Combination of the results with previous reports gives us strong indications that PA grafted  $TiO_2$  catalyzes its photo-induced oxidative degradation by promoting the formation of reactive oxygen species upon exposure to humid conditions and ambient light. These insights have implications for applications where humid conditions are applied while being exposed to ambient light. Furthermore, this knowledge can be valuable when discrepancies are found between the predicted and actual performance of PA grafted  $TiO_2$  materials. Further research is required towards the exploration of how the  $TiO_2$  support properties, in synergy with the grafted organophosphonic acid, influence the ageing kinetics, mechanism and specific interactions with water. Finally, this work provides new insights on the storage and photostability of PA grafted  $TiO_2$  in the presence of moist, creating critical awareness in the research community working on hybrid titania materials and other possible photo-active materials to evaluate changes in photo-activity and stability after surface grafting.

## Experimental

### Materials

3-Aminopropylphosphonic acid hydrochloride salt (3APPA) and propylphosphonic acid (3PPA) were purchased from Sikémia. Monomethyl-dimethylphosphate mixture (MP-DMP) and trimethylphosphate (TMP, 98%) were purchased from abcr GmbH. Orthophosphoric acid (oPA, 85%) and potassium dihydrogen phosphate (PDHP) were purchased from Sigma-Aldrich. Dipropyldiphosphonic acid (DPDPA) was purchased from SelectLab Chemicals GmbH. Different commercially available  $TiO_2$  oxide powders were studied as support: mesoporous  $TiO_2$  Hombikat M311 (Sachtleben Chemie GmbH, Venator) and high surface area rutile TIHSR (Flew Solutions).

## Surface modifications

### Surface modifications with 3APPA and 3PPA

Hombikat M311 or TIHSR was added to an aqueous 3APPA or 3PPA solution in a 2 g/50 mL solid/liquid ratio and stirred for 4 h under reflux at 50 °C. Concentrations of 20 and 150 mM were used for 3APPA and 3PPA. After modification, the samples were washed by pressure filtration (Sterlitech) to remove unreacted and physisorbed PA. During this process, the reactant solution was removed, followed by batch pressure filtration with 400 mL H<sub>2</sub>O for each washing step. After ten consecutive washing steps (i.e., a total volume of 4 L), the samples were dried overnight in an oven at 60 °C. All samples received structural names indicating the modification conditions, e.g., 3APPA20 which represents a sample modified with 20 mM of 3APPA, or 3PPA150 which represents a sample modified with 150 mM of 3PPA.

### Surface modifications with phosphate derivatives

2.0 g of Hombikat M311 was added to 50 mL of a 150 mM aqueous solution of MM-DMP, TMP, PDHP or oPA and stirred for 4 h under reflux at 50 °C. After modification, the samples were washed and dried as described previously for the 3APPA and 3PPA modifications.

### Surface modification with DPDPA

1.0 g of Hombikat M311 was added to 20 mL of a 25 mM aqueous solution of dipropyldiphosphonic acid (DPDPA) and stirred for 4 h under reflux at 90 °C. After modification, the sample was washed on a filter with 30 mL of water, and this washing procedure was repeated 3 times. Afterwards, the sample was dried overnight in an oven at 60 °C.

## Experimental set-up, ageing conditions and research strategy

### Impact of humidity during ageing

Two different atmospheric conditions were used to study the impact of humidity during storage on the surface properties of 3APPA and 3PPA modified Hombikat M311. On the one hand, the modified samples were placed in a desiccator, containing an oversaturated NaCl solution to generate and maintain a humid atmosphere with a relative humidity of 75% (wet atmosphere). On the other hand, the modified samples were sealed under argon inside a glovebox and placed in a desiccator which was being purged under a constant flow of N<sub>2</sub> (dry atmosphere). During a storage time of 495 days at ambient temperature and exposure to ambient light, samples were taken after certain time intervals to characterize possible changes in the surface properties (Table 3).

### Impact of bulk (liquid) water and different illumination conditions

Hombikat M311 and TIHSR modified with 3APPA at a concentration of 20 mM were stirred for 12 days in water at room temperature while being exposed to different illumination conditions. The UVA illumination experiments were conducted using a 18 W UVA black light lamp (TL-D 18 W BLB, Philips) at a distance of 10 cm from the aqueous dispersions. Jacketed glass cells with cooling liquid were used to avoid evaporation and to maintain the temperature of the aqueous dispersions at 20 °C. After 12 days, the samples were washed by pressure filtration and dried overnight in an oven at

**Table 3.** Overview of measurement campaigns for each characterization technique. (1) refers to the start of the study.

Days	<sup>31</sup> P NMR	<sup>13</sup> C NMR	DRIFT	XPS	ToF SIMS	Water sorption	Elemental analysis
0 (1)	✓	✓	✓		✓	✓	✓
4	✓			✓			
14	✓						
28	✓						
62	✓						
104	✓		✓				
140	✓			✓			
195	✓						
257	✓			✓	✓	✓	
313	✓						
371	✓	✓	✓	✓		✓	✓
495	✓	✓			✓	✓	✓

60 °C. As control experiments, aqueous solutions of pure 3APPA and 3PPA with a concentration of 150 mM were also stirred for 12 days under the same irradiation conditions as for the modified samples. Samples with exposure to ambient light and samples without exposure to light were prepared as references.

### Characterization of the starting support powders

Hombikat M311 and TIHSR were characterized via nitrogen sorption, SEM and XRD analyses to determine the specific surface area and pore size distribution, the particle morphology and crystal phases, respectively. The N<sub>2</sub> adsorption/desorption isotherms and pore size distributions are shown in Figure S.35. SEM images and XRD spectra are shown in Figure S.36 and Figure S.37–S.38, respectively. A summary of the determined physicochemical properties for both supports can be found in Table S.4.

### Instrumentation

Inductively Coupled Plasma Optical Emission Spectroscopy (Agilent Technologies 5100 ICP-OES) was performed to determine the phosphorus content of the grafted samples. Samples were digested in a mixture of 1.5 mL HNO<sub>3</sub> (67–69%), 1.5 mL HF (48%) and 3 mL H<sub>2</sub>SO<sub>4</sub> (96%) for 24 hours at 250 °C. After digestion, 16 mL H<sub>3</sub>BO<sub>3</sub> (4%) was added to neutralize the HF. The modification degree in number of grafted groups per nm<sup>2</sup> (#groups/nm<sup>2</sup>) was calculated from the weight percentage of phosphorus using the following formula:

$$\text{mod. degr.} \left( \frac{\#}{\text{nm}^2} \right) = \frac{\text{wt \%}(P) \times N_A}{MM(P) \times S_{\text{BET}} \times 100}$$

in which wt%(P) is the weight percentage of phosphorus in the sample, MM (P) is the molar mass of P (g/mol), S<sub>BET</sub> (nm<sup>2</sup>/g) is the surface area of the unmodified support and N<sub>A</sub> is Avogadro's constant (molecules/mol). The experimental error is estimated to be 0.1 groups/nm<sup>2</sup> based on four repeated modifications at fixed synthesis conditions. An overview of the modification degrees for Hombikat M311 grafted with 3APPA and 3PPA and the different phosphate derivatives are given in Table S.2.

Elemental analyses on carbon and nitrogen were performed on a Vario EL Cube CHNS elemental analyzer (Elementar), equipped with

a TCD detector. A sample intake of 15–20 mg was used for each measurement, using tin boats (4×4×11 mm) as sample cup. The samples were burned in an oxygen-rich environment and the combustion tube was set at a temperature of 1150 °C. Before each measurement, calibration and control measurements were performed with sulfanilamide and sulfanilic acid, respectively.

To study the impact of ageing at the level of the phosphonate moiety of 3APPA and 3PPA grafted TiO<sub>2</sub>, <sup>31</sup>P-MAS (Magic Angle Spinning) solid-state NMR spectra were acquired at ambient temperature on an Agilent VNMRS DirectDrive 400 MHz spectrometer (9.4 Tesla wide bore magnet) equipped with a T3HX 3.2 mm VT probe. Magic angle spinning was performed at 15 kHz using ceramic zirconia rotors of 3.2 mm in diameter (22 μL rotors). The phosphorus chemical shift scale was calibrated to KH<sub>2</sub>PO<sub>4</sub> at 3.9 ppm. Other acquisition parameters used were: a spectral width of 60 kHz, a 90° pulse length of 3.2 μs, an acquisition time of 15 ms, a recycle delay time of 204 s and around 512 accumulations. High power proton dipolar decoupling during the acquisition time was set at 80 kHz.

To study the impact of ageing at the level of the carbon chain of 3APPA and 3PPA grafted TiO<sub>2</sub>, <sup>13</sup>C-CPMAS solid-state NMR spectra were acquired on a Bruker 400 MHz spectrometer (9.4 Tesla wide bore magnet) with a 4 mm MASVT BL4 X/Y/H probe. Magic angle spinning was performed at 10 kHz. The aromatic signal of hexamethylbenzene was used to calibrate the Hartmann-Hahn condition for CP and the carbon chemical shift scale (132.1 ppm). Acquisition parameters used were: a spectral width of 50 kHz, a 90° pulse length of 4.0 μs, an acquisition time of 20 ms, a recycle delay time of 2.5 s, a spin-lock field of 50 kHz, a contact time of 1.0 ms and 30000–150000 accumulations. High power proton dipolar decoupling during acquisition was set to 80 kHz.

Detailed molecular and elemental insights into possible changes in the chemical composition and surface interactions were obtained by ToF-SIMS measurements. These were acquired with a ToF.SIMS 5 system from ION-TOF GmbH (Münster, Germany), using a 30 keV Bi<sup>3+</sup> primary ion beam in high current bunched mode for a high mass resolution (0.70 pA target current, 3 μm lateral resolution). Analysis areas of 100 μm×100 μm were raster-scanned (128×128 pixels) to obtain either positive or negative secondary ion mass spectra. The primary ion dose was kept below the static limit of 1×10<sup>13</sup> ions cm<sup>-2</sup> analysis<sup>-1</sup>. The pressure in the ToF-SIMS main chamber was ~3.5×10<sup>-8</sup> mbar during measurements. In the overlays presented within the main text and SI, the C<sub>2</sub>H<sub>2</sub>O<sub>4</sub>Ti<sup>-</sup>, C<sub>2</sub>HO<sub>2</sub>Ti<sup>-</sup> and SiCH<sub>3</sub>O<sub>2</sub>Ti<sup>-</sup> fragments were surface contaminants since they were already present on the native support.

To investigate the impact of phosphonic acid grafting on the intrinsic reactivity of the surface towards the formation of radical species and intermediates, X-band continuous wave (CW)-EPR measurements were performed on a Bruker Elexsys E580 spectrometer at a microwave frequency of ~9.68 GHz, with a microwave power of 2 mW. The modulation frequency is 100 kHz and the modulation amplitude is 0.1 mT. The measurements were first performed in air. Subsequently, the samples were degassed under a high vacuum (<10<sup>-4</sup> mbar) for a second series of measurements. Spectra were simulated using EasySpin, an open-source MATLAB toolbox (MathWorks, Natick, Mass., USA).<sup>[45]</sup>

## CRedit authorship contribution statement

**Nick Gys:** Conceptualization, Methodology, Validation, Investigation, Writing-original draft, Visualization. **Bram Pawlak (NMR):** Conceptualization, Methodology, Validation, Investiga-

tion, Writing-original draft, Visualization. **Kristof Marcoen (ToF-SIMS):** Methodology, Validation, Investigation, Writing-original draft, Visualization. **Gunter Reekmans (NMR):** Methodology, Validation, Investigation. **Leticia F. Velasco (Water sorption):** Validation, Investigation, Writing-original draft, Visualization. **Rui An (EPR):** Methodology, Investigation, Validation, Visualization. **Kenny Wyns:** Investigation. **Kitty Baert (XPS):** Methodology, Investigation, Validation. **Kaimin Zhang:** Investigation, Validation. **Léon Luntadila Lufungula:** Investigation, Validation. **Alessandra Piras:** Investigation, Validation. **Laurens Siemons:** Investigation, Validation. **Sabine Van Doorslaer (EPR):** Methodology, Validation, Writing-review & editing. **Bart Michiels:** Writing-review & editing, Supervision. **Frank Blockhuys (DFT calculations):** Methodology, Validation, Investigation, Writing-review & editing, Visualization, Supervision. **Tom Hauffman (XPS):** Conceptualization, Methodology, Writing-review & editing, Supervision. **Peter Adriaensens (NMR):** Conceptualization, Methodology, Writing-review & editing, Supervision. **Steven Mullens:** Conceptualization, Methodology, Writing-review & editing, Supervision. **Vera Meynen:** Conceptualization, Methodology, Writing-review & editing, Supervision.

## Acknowledgements

*This work is supported by the Research Foundation Flanders (FWO) and Hasselt University via the Hercules project AUHL/15/2-GOH3816N. K. Zhang is supported by the EASiCHEM project funded by the Flemish Strategic Basic Research Program of the Catalisti cluster and Flanders Innovation & Entrepreneurship (HBC.2018.0484). B. Pawlak acknowledges the FWO project G. 0121.17N and Rui An is grateful for the DOCPRO4 bonus project of the University of Antwerp. V. Meynen acknowledges the Research Foundation-Flanders (FWO) for project K801621N. EPR measurements were performed in the UAntwerp EPR facility funded by FWO (grant 1004920N to S. Van Doorslaer and V. Meynen). All calculations were performed using the Hopper HPC infrastructure at the CalcUA core facility of the University of Antwerp, a division of the Flemish Supercomputer Center VSC, funded by the Hercules Foundation, the Flemish Government (department EWI) and the University of Antwerp. The authors would like to acknowledge Jef De Wit for the CHNS analysis, Wilfried Brusten and Filip Beutels for the ICP measurements, Saskia Defossé and Karen Leyssens for the N<sub>2</sub> sorption measurements, Raymond Kempers for the SEM measurements, Y.H. Vincent Ching for help with the EPR measurements and Myrjam Mertens for the XRD measurements.*

## Conflict of Interest

*The authors declare no conflict of interest.*

## Data Availability Statement

The raw and processed data required to reproduce these findings will be made available upon request to the authors.

**Keywords:** ageing · organophosphonic acids · photo-oxidation · surface chemistry · titanium dioxide

- [1] C. Queffelec, M. Petit, P. Janvier, D. A. Knight, B. Bujoli, *Chem. Rev.* **2012**, *112*, 3777–3807.
- [2] G. Guerrero, J. G. Alauzun, M. Granier, D. Laurencin, P. H. Mutin, *Dalton Trans.* **2013**, *42*, 12569–12585.
- [3] A. Roevens, J. G. Van Dijk, M. Tassi, J. D'Haen, R. Carleer, P. Adriaensens, F. Blockhuys, V. Meynen, *Mater. Chem. Phys.* **2016**, *184*, 324–334.
- [4] M. Tassi, G. Reekmans, R. Carleer, P. Adriaensens, *Solid State Nucl. Magn. Reson.* **2016**, *78*, 50–55.
- [5] A. Roevens, J. G. Van Dijk, D. Geldof, F. Blockhuys, B. Prelot, J. Zajac, V. Meynen, *Appl. Surf. Sci.* **2017**, *416*, 716–724.
- [6] M. Tassi, A. Roevens, G. Reekmans, M. Vanhamel, V. Meynen, J. D'Haen, P. Adriaensens, R. Carleer, *Adv. Powder Technol.* **2017**, *28*, 236–243.
- [7] R. B. Merlet, M. A. Pizzoccaro-Zilamy, A. Nijmeijer, L. Winnubst, *J. Membr. Sci.* **2020**, *599*, 117839.
- [8] G. Mustafa, K. Wyns, P. Vandezande, A. Buekenhoudt, V. Meynen, *J. Membr. Sci.* **2014**, *470*, 369–377.
- [9] A. Mitrofanov, S. Brandès, F. Herbst, S. Rigolet, A. Bessmertnykh-Lemeune, I. Beletskaya, *J. Mater. Chem. A* **2017**, *5*, 12216–12235.
- [10] F. Forato, A. Belhoub, J. Monot, M. Petit, R. Benoit, V. Sarou-Kanian, F. Fayon, D. Jacquemin, C. Queffelec, B. Bujoli, *Chem. A Eur. J.* **2018**, *24*, 2457–2465.
- [11] J. Zhang, S. Deo, M. J. Janik, J. Will Medlin, *J. Am. Chem. Soc.* **2020**, *142*, 5184–5193.
- [12] M. A. Pizzoccaro-Zilamy, S. M. Piña, B. Rebiere, C. Daniel, D. Farrusseng, M. Drobek, G. Silly, A. Julbe, G. Guerrero, *RSC Adv.* **2019**, *9*, 19882–19894.
- [13] M. Abdellah, A. M. El-Zohry, L. J. Antila, C. D. Windle, E. Reisner, L. Hammarström, *J. Am. Chem. Soc.* **2017**, *139*, 1226–1232.
- [14] H. Chen, W. Zhang, M. Li, G. He, X. Guo, *Chem. Rev.* **2020**, *120*, 2879–2949.
- [15] S. A. Paniagua, A. J. Giordano, O. L. Smith, S. Barlow, H. Li, N. R. Armstrong, J. E. Pemberton, J. L. Brédas, D. Ginger, S. R. Marder, *Chem. Rev.* **2016**, *116*, 7117–7158.
- [16] N. Riboni, C. Spadini, C. S. Cabassi, F. Bianchi, S. Grolli, V. Conti, R. Ramoni, F. Casoli, L. Nasi, C. de Julián Fernández, P. Luches, M. Careri, *RSC Adv.* **2021**, *11*, 11256–11265.
- [17] N. Knežević, I. Gadjanski, J. O. Durand, *J. Mater. Chem. B* **2019**, *7*, 9–23.
- [18] G. A. Seisenbaeva, I. V. Melnyk, N. Hedin, Y. Chen, P. Eriksson, E. Trzop, Y. L. Zub, V. G. Kessler, *RSC Adv.* **2015**, *5*, 24575–24585.
- [19] Q. A. Trieu, S. Pellet-Rostaing, G. Arrachart, Y. Traore, S. Kimbel, S. Daniele, *Sep. Purif. Technol.* **2020**, *237*, 116353.
- [20] P. H. Mutin, G. Guerrero, A. Vioux, *J. Mater. Chem.* **2005**, *15*, 3761–3768.
- [21] F. Brodard-severac, G. Guerrero, J. Maquet, P. Florian, C. Gervais, P. H. Mutin, I. Charles, G. Montpellier, V. Uni, M. Curie, V. Uni, *Chem. Mater.* **2008**, *20*, 5191–5196.
- [22] D. Geldof, M. Tassi, R. Carleer, P. Adriaensens, A. Roevens, V. Meynen, F. Blockhuys, *Surf. Sci.* **2017**, *655*, 31–38.
- [23] J. W. Blanchard, T. L. Groy, J. L. Yarger, G. P. Holland, *J. Phys. Chem. C* **2012**, *116*, 18824–18830.
- [24] N. Gys, L. Siemons, B. Pawlak, K. Wyns, K. Baert, T. Hauffman, P. Adriaensens, F. Blockhuys, B. Michielsen, S. Mullens, V. Meynen, *Appl. Surf. Sci.* **2021**, *566*, 150625.
- [25] M. Wagstaffe, A. G. Thomas, M. J. Jackman, M. Torres-Molina, K. L. Syres, K. Handrup, *J. Phys. Chem. C* **2016**, *120*, 1693–1700.
- [26] N. Kyriakou, M. A. Pizzoccaro-Zilamy, A. Nijmeijer, M. Luiten-Olieman, L. Winnubst, *Microporous Mesoporous Mater.* **2020**, *307*, 110516.
- [27] M. Kosian, M. M. J. Smulders, H. Zuilhof, *Langmuir* **2016**, *32*, 1047–1057.
- [28] S. Marcinko, A. Y. Fadeev, *Langmuir* **2004**, *20*, 2270–2273.
- [29] G. Guerrero, P. H. Mutin, A. Vioux, *Chem. Mater.* **2001**, *13*, 4367–4373.
- [30] A. Bachinger, G. Kickelbick, *Appl. Catal. A* **2011**, *409–410*, 122–132.
- [31] G. Fiscaro, S. Filice, S. Scalese, G. Compagnini, R. Reitano, L. Genovese, S. Goedecker, I. Deretzis, A. La Magna, *J. Phys. Chem. C* **2020**, *124*, 2406–2419.
- [32] J. G. Van Dijck, H. Lenaerts, L. Siemons, F. Blockhuys, V. Meynen, *Surfaces and Interfaces* **2020**, *21*, 100710.
- [33] R. M. Silverstein, F. X. Webster, D. J. Kiemle, *Spectrometric Identification of Organic Compounds*, John Wiley & Sons, Inc, **2005**.
- [34] G. Socrates, *Infrared and Raman Characteristic Group Frequencies*, **2004**.
- [35] E. Carter, A. F. Carley, D. M. Murphy, *ChemPhysChem* **2007**, *8*, 113–123.
- [36] V. Rahemi, S. Trashin, Z. Hafideddine, S. Van Doorslaer, V. Meynen, L. Gorton, K. De Wael, *Anal. Chem.* **2020**, *92*, 3643–3649.
- [37] D. A. H. Hanaor, C. C. Sorrell, *J. Mater. Sci.* **2011**, *46*, 855–874.
- [38] J. Y. Hwang, G. hee Moon, B. Kim, T. Tachikawa, T. Majima, S. Hong, K. Cho, W. Kim, W. Choi, *Appl. Catal. B* **2021**, *286*, 119905.
- [39] Y. Nosaka, A. Nosaka, *ACS Energy Lett.* **2016**, *1*, 356–359.
- [40] L. Ding, M. Li, Y. Zhao, H. Zhang, J. Shang, J. Zhong, H. Sheng, C. Chen, J. Zhao, *Appl. Catal. B* **2020**, *266*, 118634.
- [41] K. Shirai, G. Fazio, T. Sugimoto, D. Selli, L. Ferraro, K. Watanabe, M. Haruta, B. Ohtani, H. Kurata, C. Di Valentin, Y. Matsumoto, *J. Am. Chem. Soc.* **2018**, *140*, 1415–1422.
- [42] A. Litke, Y. Su, I. Tranca, T. Weber, E. J. M. Hensen, J. P. Hofmann, *J. Phys. Chem. C* **2017**, *121*, 7514–7524.
- [43] F. Liu, N. Feng, Q. Wang, J. Xu, G. Qi, C. Wang, F. Deng, *J. Am. Chem. Soc.* **2017**, *139*, 10020–10028.
- [44] Z. Wang, A. Mahmood, X. Xie, X. Wang, H. Qiu, J. Sun, *Chem. Eng. J.* **2020**, *393*, 124723.
- [45] S. Stoll, A. Schweiger, *J. Magn. Reson.* **2006**, *178*, 42–55.

Manuscript received: December 5, 2022  
Revised manuscript received: February 13, 2023  
Accepted manuscript online: February 19, 2023